

# Accurate Stereo Matching using the Pixel Response Function

## Abstract

The comparison of intensity is inevitable in almost all computer vision applications. Since the recorded intensity values are dependent on the camera and its noise characteristic, the traditional intensity-based similarity measurements suffer from inaccuracy between images taken by different cameras. To overcome these difficulties, we calculate the similarity measure in the scene radiance space by using the Inverse Radiometric Response Function (IRRF). Previously, IRRF was assumed to be spatially invariant, however, the pixel-wise differences served as hindrances in accurately measuring scene radiance on two different images. Accordingly, we define a pixel-wise IRRF as the Inverse Pixel Response Function (IPRF). The paper seeks to prove that the stereo matching in the scene radiance space works accurately in different camera settings in which conventional methods fail.

## 1. Introduction

Many computer vision problems including stereo matching and dense 3D reconstruction, deal with two or more images. Calculating the similarity between pixels in different images, we usually assume that the input images' statistics are not much different, or are sophisticatedly refined such as the Middlebury stereo datasets [2]. However, if we take the pictures of images using different cameras, the image statistics yield varied results which seriously contaminate conventional  $L_p$  norm-based similarity measures such as Sum of Absolute Difference (SAD), Sum of Squared Difference (SSD), and Birchfield-Tomasi (BT). To purify the contaminated measures, Normalized Cross Correlation (NCC) was proposed early in the literature, especially to the stereo matching problem [5] and further related works were proposed to deal with similarity measure under different image conditions: mutual information (MI) [12] and conventional Birchfield-Tomasi (BT) data cost with various preprocessing techniques: LoG, Rank, and Mean filtered

images [11].

In this paper, we adopt a direct approach to correct camera variations between images through the pixel-wise radiometric response function named Pixel Response Function (PRF) so as to enhance the accuracy of data cost for the MAP-MRF stereo problem. Previously, Radiometric Response Function (RRF) was generally assumed to be spatially invariant [9]. However, since CCD pixels have slightly different gains and offsets by their own amplifiers [23] and lens characteristic is also spatially inhomogeneous [20], the RRF varies spatially. Therefore, we eliminate the assumption and define the more precise RRF as the PRF. To obtain the PRF, we measure each pixel's intensity characteristic that depends on reference intensity values. For the stereo matching application, we apply our approach to data cost by the Inverse PRF (IPRF) and obtain enhanced results. Main contribution of this paper is to radiometrically normalize two images by the IPRF in pixel precision so that the similarity measure between images under different camera settings can be accurately corrected.

In the following sections, we introduce radiometric calibration and its pixel-wise extension in detail and standard MAP-MRF stereo framework for an application. Finally, we present experimental results to show the accurate stereo results in different camera settings through our approach.

### 1.1. Radiometric Calibration

The radiometric calibration is to find the radiometric response function (RRF) denoted by  $F(L)$ . The RRF maps scene radiance value  $L$  to image intensity  $B$  and is a composite function of the camera response function (CRF)  $f_{\text{CRF}}(E)$  for a CCD irradiance  $E$  and a linear function  $s(L)$  [8] by

$$\begin{aligned} B &= F(L) = f_{\text{CRF}}(E), \\ E &= s(L). \end{aligned} \tag{1}$$

The CRF represents CCD characteristic of digital camera or film characteristic of film camera and the linear function  $s(L)$  represents optical characteristics of camera lens including vignetting and lens fall-off [8].

The radiometric calibration study was started in early 1990s [10]. At the beginning, radiomet-

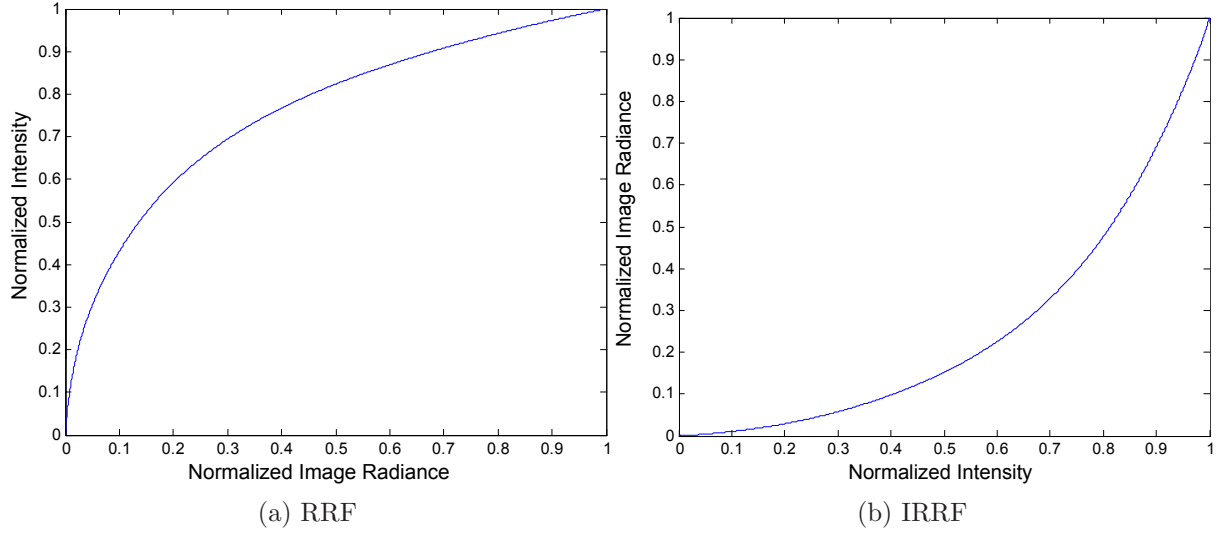


Figure 1. Example of RRF and IRRF

ric calibration researches mainly focused on recovering a high dynamic ranged scene with differently exposed images [4]. Similarly, Mitsunaga and Nayar devised an algorithm to accurately reconstruct the Inverse RRF, IRRF, using differently exposed images [19]. Since Mitsunaga and Nayar’s method was considered accurate, the subsequent works focused on new methods to obtain IRRF. For instance, Lin et al. utilized the linearity of color space in a single color image [14] and the edge smoothness in a single grayscale image [15] and Matsushita recently used noise distribution [18].

In the following sections, we try to use the IRRF to recover scene radiance values for the stereo matching.

## 2. Radiometric Calibration for Stereo Matching

Since our goal is to obtain a scene radiance value from image intensity, we need to obtain the IRRF rather than the RRF as shown in Fig. 1. In the following subsection, under the assumption that both the linear function  $s(L)$  and the CRF  $f_{\text{CRF}}(E)$  are spatially invariant [18, 14, 19, 8, 10, 15, 9], we show that the similarity measure between images taken by different cameras is impaired and it is recovered by each IRRF as depicted in Fig. 3, i.e.  $d(A) > d(B)$  where  $d(x)$  is Euclidean distance of  $x$ .

### 2.1. Spatially Invariant Radiometric Response Function

Since the linear function  $s(L)$  is also assumed to be spatially homogenous for a certain camera, we can assume that the linear function in (1) is 1 to make the CRF as the RRF directly for

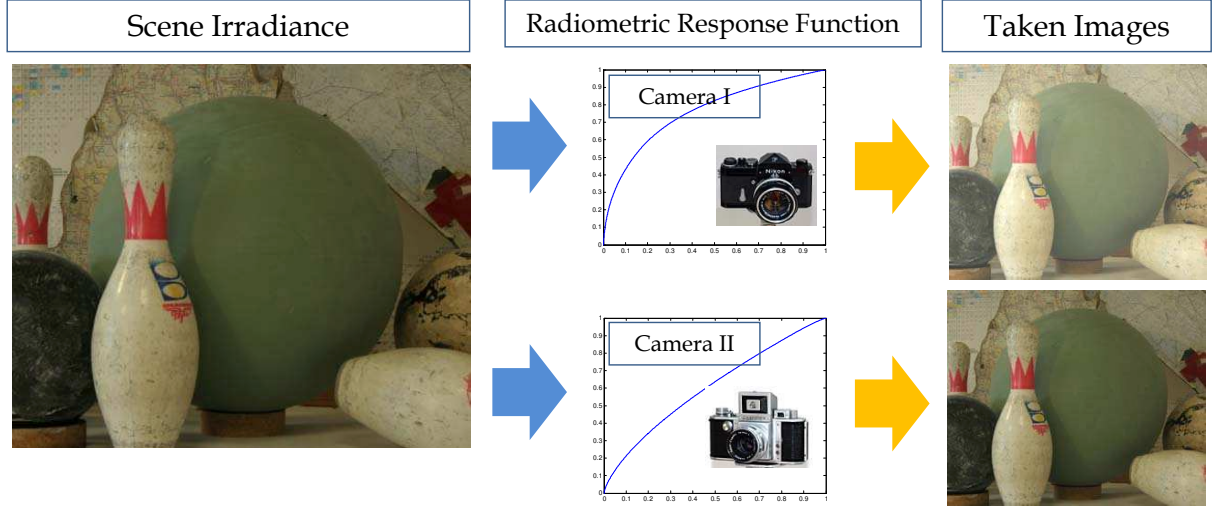


Figure 2. Transform with different RRFs

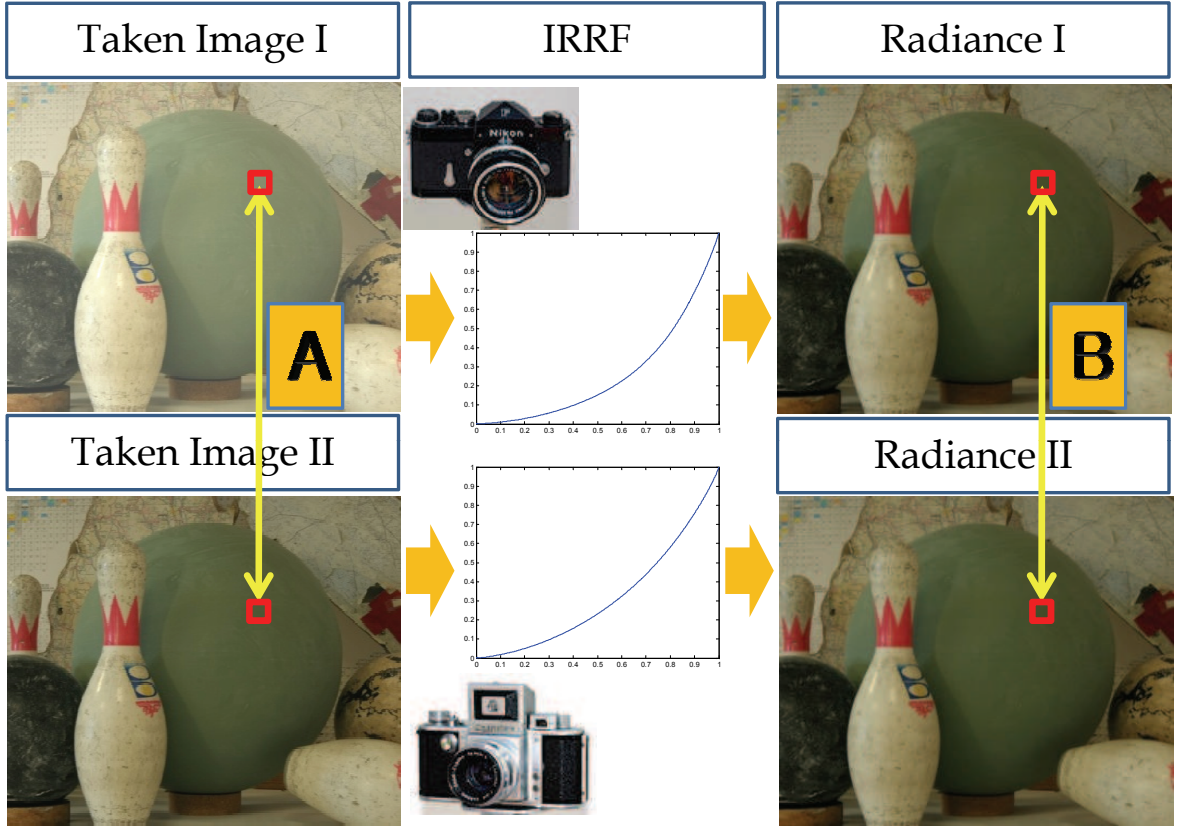
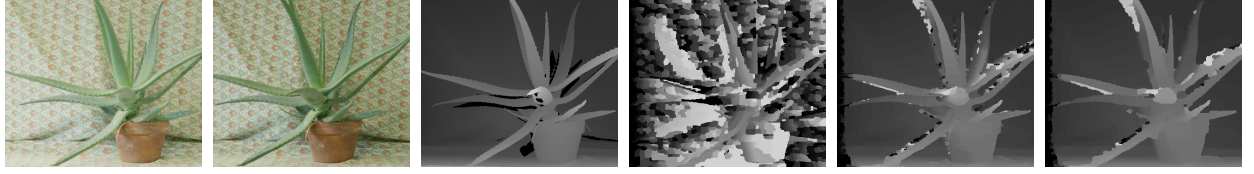


Figure 3. Radiance recovery using each IRRFs

convenience. Thus when we apply the IRRF, we can recover a scene radiance value from image intensity and obtain accurate similarity measure in the scene radiance space as shown in Fig. 3.

To illustrate the camera variation between images dramatically, we transform the left and the right images of the refined Middlebury dataset with the well-known CRF database named DoRF of Columbia CAVE [1] as shown in Fig. 2. We assume that the Middlebury dataset is



(a) Left Image (b) Right Image (c) GND Truth (d) Intensity-BT (e) HE Intensity-BT (f) IRRF-BT  
Figure 4. Results of Middlebury Stereo Dataset by Different Camera. (a) is the left image taken by Agfa Color-FuturaII 200CDBLue (b) is the right image taken by Agfa Color HDC 100PlusCDGreen (c) is ground truth (d) Disparity map by BT cost in the intensity space (e) Disparity map by BT in the intensity space with normalization by histogram equalization (f) Disparity map by BT in the scene radiance space by IRRF recovery

perfectly refined, though it is not true. Now, we can show that the traditional  $L_p$  similarity measure between images taken by different cameras is no longer valid as we can notice that the subsequent stereo result using  $L_p$ -norm based BT cost is seriously harmed as shown in Fig. 4(d). To ameliorate the similarity measure before we restore it by each IRRF, we use histogram equalization which is one of the widely used image normalization techniques (HE). Though the result is alleviated by HE, radiometric calibration gives the better result through recovered scene radiance Fig. 4(e) and 4(f). The reason why the result of Fig. 4(f) is not the same to the ground truth is because that the assumption that the Middlebury dataset is perfectly refined is wrong and both the BT data cost and the MAP-MRF framework is not the best in the stereo matching [11]. To verify that using the IRRF enhances data cost for the stereo matching rather than image normalization, we quantitatively analyze the stereo matching results by the error pixel ratio<sup>1</sup> for several Middlebury stereo data in Table 1.

Table 1. Error pixel ratio of Middlebury dataset transformed by different cameras (%)

	aloe	bowling1	midd1
Intensity-based BT	88.9	95.9	92.8
HE Intensity-based BT	20.6	74.3	58.3
IRRF-based BT	18.3	51.7	56.4

Assuming that the IRRF is spatially invariant, we can ignore the pixel-wise variations between two different images. Since the homogeneity assumption of IRRF is not correct, we are going to verify the pixel-wise difference and eliminate the assumption by obtaining radiometric response for each pixel.

<sup>1</sup>The error pixel ratio is defined by a ratio of the number of pixels which have disparity difference with ground truth greater than 1 to the total number of pixels in the image. [21]

## 2.2. Pixel Response Function

The pixel variations come from a camera itself and environmental conditions outside the camera - air condition, fog, and rain. In this paper, assuming that we take pictures in good weather condition, we model the variations originated only from a camera itself for simplicity.

The variations from the camera is also composed of two parts: one is the time-invariant variations that we want to find out and another is the time-varying noise perturbation such as CCD thermal noise, fixed pattern noise, dark current noise, and shot noise [16]. Since it is hard to model the time-varying noise, we only consider the time-invariant variations. To obtain the variations without the effect of noise, we model the pixel's intensity response distribution by a Gaussian noise model, because the distribution has been plausibly modelled by a Gaussian model [17, 18].

**Gaussian Noise Model** A Gaussian model has two parameters, namely, the mean and the variance. The mean is regarded as a statistically reliable true value, while the variance is considered as a perturbation caused by the noise [16].

To obtain the intensity response distribution for a pixel as shown in Fig. 5, we take multiple shots of static scene. In this paper, we use 2,000 shots for a scene to obtain the distribution. By taking the mean value of the distribution for each pixel, we obtain the noiseless intensity for a pixel denoted as  $B(x, y)$  as shown in Fig. 6.

### 2.2.1 Pixel Variation by a Single Gain

To model the noiseless pixel variations, we consider the CCD variations and the optical characteristics of lens. The CCD variations are composed of the intensity dependent gain and the intensity independent offset [23]. The optical characteristics, such as vignetting and lens fall-off, represented by a scene radiance dependent gain [20]. Since we cannot know the scene radiance value to obtain the noiseless pixel variations, we assume that the scene radiance dependent optical gain is dependent on the image intensity for simplicity. Considering the CCD gain  $R_{\text{CCD}}(x, y, B)$ , optical gain  $R_{\text{OPT}}(x, y, B)$ , and the CCD offset  $\delta B(x, y)$  versus the variation-free intensity value  $B$ , we write the modelled noiseless intensity of a pixel position  $(x, y)$  is by

$$B(x, y) = (R_{\text{CCD}}(x, y, B) + R_{\text{OPT}}(x, y, B)) \cdot B + \delta B(x, y). \quad (2)$$

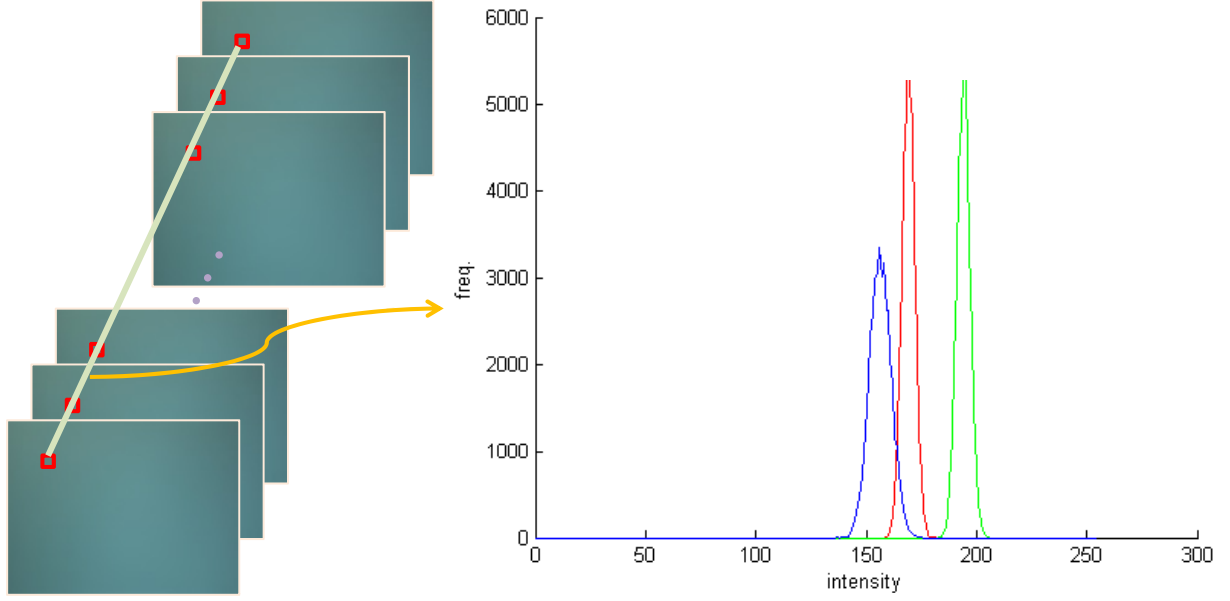
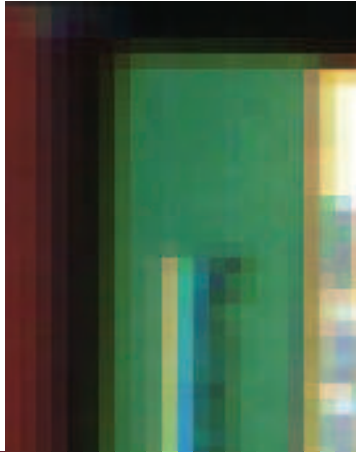


Figure 5. Intensity varying distribution of a pixel  $(x, y)$ ,  $B(x, y)$ . A pixel in multiple shots shows intensity distribution similar to Gaussian distribution. The red, blue, and green lines show the distribution of each color channel. We can obtain noiseless intensity value for the pixel by taking mean of the intensity distribution.



(a) Original Image



(b) Noiseless Image

Figure 6. Noisy image and noiseless image by calculating intensity mean for a pixel of multiple shots.

To simplify (2), we can rewrite the equation with a single gain denoted as  $R(x, y, B)$  by

$$B(x, y) = R(x, y, B) \cdot B, \quad (3)$$

where the gain  $R(x, y, B)$  of a pixel  $(x, y)$  is a pixel variation that we want to obtain and is defined as a ratio of the observed intensity to the variation-free intensity  $B$ :  $R(x, y, B) = \frac{B(x, y)}{B}$ .



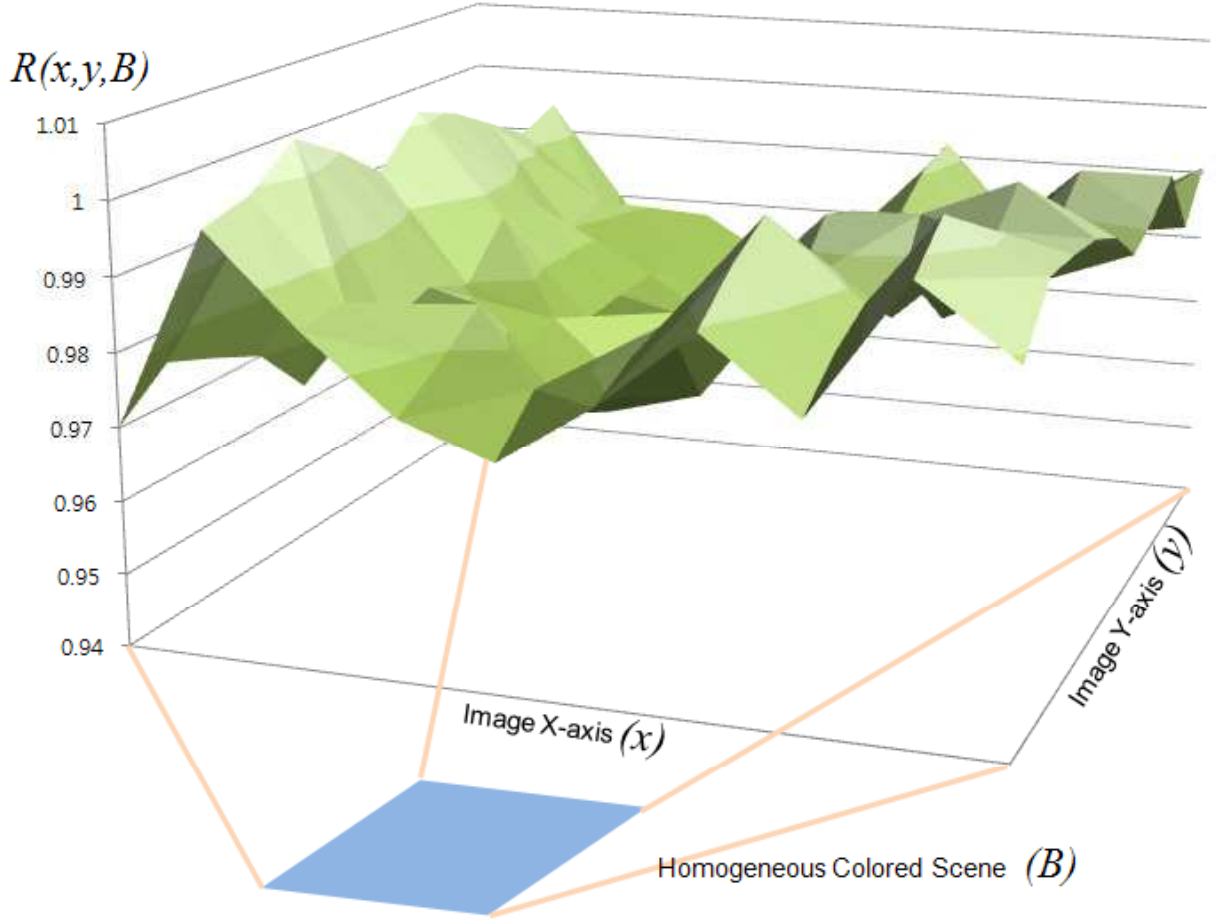


Figure 7. Noiseless pixel variation of a homogeneous scene. The noiseless single gain  $R(x, y, B)$  of each pixel  $(x, y)$  in  $10 \times 10$  homogeneous colored image patch in (4) is illustrated.

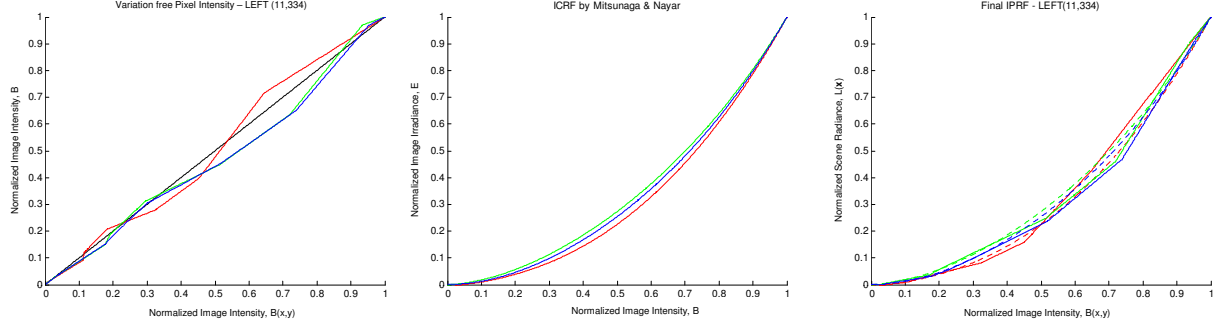
It incorporates all the variations for a pixel from a camera by

$$R(x, y, B) = R_{\text{CCD}}(x, y, B) + R_{\text{OPT}}(x, y, B) + \frac{\delta B(x, y)}{B}. \quad (4)$$

To obtain the single gain  $R(x, y, B)$  of a pixel  $(x, y)$  for all  $B$  values, we obtain entire  $\frac{B(x, y)}{B}$  values for all  $B$  values from 0 to 255 by taking homogeneous colored scene. As a homogeneous colored scene, we use cloudless sky, since the scene radiance value of cloudless sky is assumed to be invariant within an image [7]. The variation-free intensity  $B$  is obtained by the mean value of the homogeneous colored sky under the assumption that the image is ergodic. We take differently exposed images to obtain  $R(x, y, B)$  for each  $B$  by adjusting camera parameters. Fig. 7 shows the pixel variation by a single gain  $R(x, y, B)$  of  $10 \times 10$  image patch for illustration.

**Linear Interpolation** In practice, however, since it is hard to obtain all  $R(x, y, B)$  values for all variation-free intensity values  $B$ , we sample 7 values for 7  $B$  values and linearly interpolate





(a) Variation-free intensity  $B$  versus  
Noiseless  $B(x, y)$

(b) ICRF

(c) IPRF

Figure 8. Obtained IPRF of a pixel. Color denotes the response of each color channel. (a) Interpolated recovering function of pixel variation free intensity  $B$  of pixel  $(x, y)$  versus observed intensity value  $B(x, y)$ . (b) ICRF for that camera obtained by Mitsunaga and Nayar’s method [19]. (c) IPRF as defined by (5). Dotted color lines denote the ICRF for comparison with the IPRF which is denoted by solid lines. This figure is not obtained from Bumblebee 1. For the illustration purpose, we use the CRF which has distinctive curved shape.

them to recover  $R(x, y, B)$  for all intensity values. Fig. 8(a) shows the variation-free intensity  $B$  from the observed intensity  $B(x, y)$  by using linearly interpolated  $R(x, y, B)$ .

### 2.2.2 Recovering Scene Radiance without Pixel Variation

Finally, we can recover scene radiance for a pixel considering pixel-wise variation using ICRF  $f_{\text{CRF}}^{-1}(B)$  for an obtained  $B$  from  $R(x, y, B)$  by

$$L(x, y) = f_{\text{CRF}}^{-1}\left(\frac{B(x, y)}{R(x, y, B)}\right). \quad (5)$$

Fig. 8(c) shows the obtained IPRF by a composition function of ICRF and the pixel variations. We illustrate that the IPRF of each pixel is different from other pixels in another image and even in the same image by Fig. 9.

## 3. Data Cost of Standard MAP-MRF Stereo Framework

The resulting scene radiance value is used as a data term for MAP-MRF stereo framework. However, if we use noisy observed intensity as a noiseless  $B(x, y)$  with some errors, still the IPRF works, though the results is somewhat deteriorated. In this paper, we use standard MAP-MRF stereo energy model represented by

$$E(l) = E_d(l) + \lambda E_s(l), \quad (6)$$

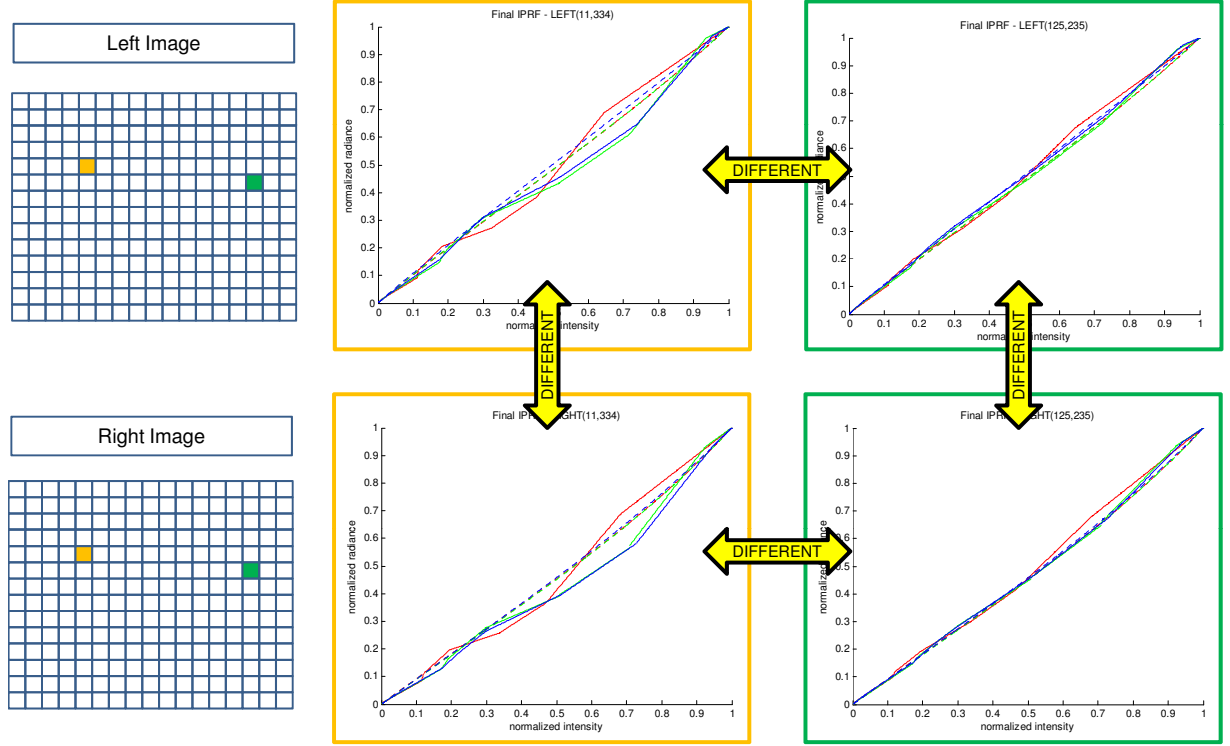


Figure 9. Difference of IPRF for each pixel. The graph in the yellow box shows IPRF for yellow pixel and the graph in green is for green pixel. The pixel-wise IRRF named IPRF is different from each other. Thus the assumption that the IRRF is spatially invariant is wrong. Dotted color lines are ICRF of the camera for comparison with IPRF. This figures are obtained from Bumblebee 1.

where  $E_d$  is a data cost,  $E_s$  is a smoothness cost, and  $l$  is a disparity value [6]. The data cost  $E_d(l)$  is variously defined by BT and NCC-based on the distance measure  $d(P_L(x, y), P_R(x, y + l(x, y)))$  which is defined between the pixel value in the left image  $I$ ,  $P_L(x, y)$ , and the pixel value in the right image,  $P_R(x + l(x, y), y)$ , with disparity  $l(x, y)$  [3] by

$$E_d(l) = \sum_{(x,y) \in I} d(P_L(x, y), P_R(x + l(x, y), y)), \quad (7)$$

We enhance the stereo matching results by calculating the data costs in the scene radiance space by the IPRF and compare them to the results of data costs in the original intensity space and the image irradiance by the ICRF. Thus, we need to obtain the data costs in each space.

If we want to define the data cost in the intensity space, we simply substitute  $P_L(x, y)$  by intensity  $B_L(x, y)$  for the left image and  $P_R(x + l(x, y), y)$  by intensity  $B_R(x + l(x, y), y)$  for the right image.

For the data cost in the image irradiance space to obtain better stereo result, we substitute  $P_L(x, y)$  and  $P_R(x + l(x, y), y)$  by the image irradiance values  $E_L(x, y)$  and  $E_R(x + l(x, y), y)$



(a) Left Image

(b) Right Image

Figure 10. Bumblebee Stereo Data 1 - Bookshelf 1 set

respectively. The image irradiance values  $E_L(x, y)$  and  $E_R(x + l(x, y), y)$  are obtained by  $f_{\text{CRF,LEFT}}^{-1}(B_L(x, y))$  and  $f_{\text{CRF,RIGHT}}^{-1}(B_R(x + l(x, y), y))$  which are ICRFs for the left and the right cameras, respectively.

Analogously, for the data cost in the scene radiance space for the best stereo result, we substitute  $P_L(x, y)$  and  $P_R(x + l(x, y), y)$  by  $L_L(x, y)$  and  $L_R(x + l(x, y), y)$ , respectively. The scene radiance value  $L_L(x, y)$  and  $L_R(x + l(x, y), y)$  are recovered scene radiance by the IPRF defined by (5) for pixel  $(x, y)$  in the left image and  $(x + l(x, y), y)$  in the right image.

Spatially smoothness constraint of disparity labels between neighboring pixels is used as smoothness cost  $E_s$  in (6) by

$$E_s(l) = \sum_{\{(x,y) \in I\}} \sum_{\{(x,y)_j \in N(x,y)\}} w_{(x,y)(x,y)_j} V(l(x, y), l(x, y)_j), \quad (8)$$

where  $N(x, y)$  is a set of the neighboring pixels of  $(x, y)$ , and  $V(l(x, y), l(x, y)_j)$  is a smoothness measure defined in [21]. In (8),  $w_{(x,y)(x,y)_j}$  is a weight of smoothness between disparity label  $l(x, y)$  and  $l_{(x,y)_j}$  of the pixel  $(x, y)$  and that of its neighborhood. Since the smoothness property should be the same while the data cost is modified, we decide to use this smoothness cost without modification.

Using two representative data costs such as BT and NCC in each space, we obtain the stereo results in the following section.



(a) Left Image



(b) Right Image

Figure 11. Bumblebee Stereo Data 2 - Bookshelf 2 set



(a) Left Image



(b) Right Image

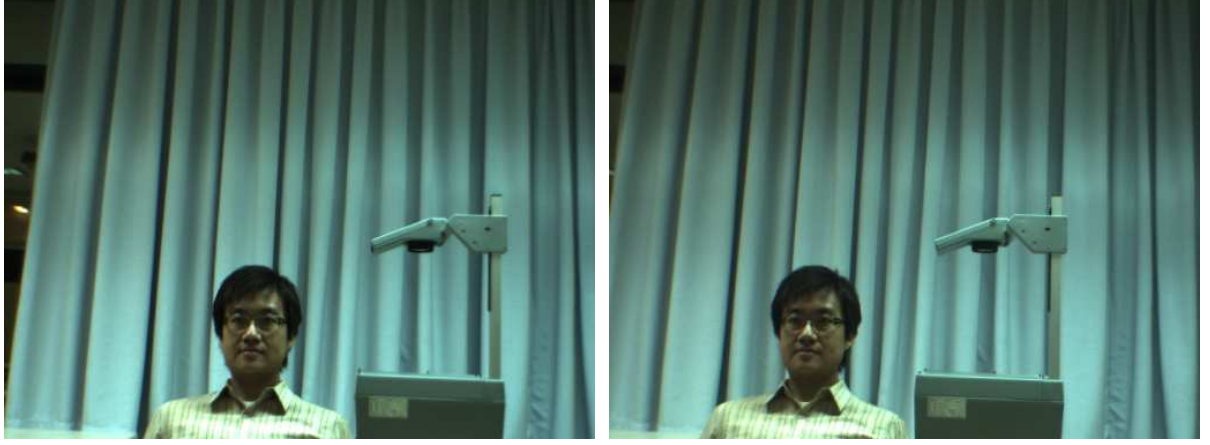
Figure 12. Bumblebee Stereo Data 3 - Photoboard set

#### 4. Experimental Results

For the experiments, we use Point Grey Research’s Bumblebee stereo vision camera. To obtain the IPRF, we need to obtain the ICRF for left and right camera of it, first. The ICRFs for both the left and the right cameras are obtained by Mitsunaga and Nayar’s method [19] with differently exposed multiple images. In addition, we calculate the noiseless pixel variation  $\frac{B(x,y)}{B}$  of each pixel  $(x, y)$  over all  $B$ s by taking multiple shots of cloudless sky.

With the obtained ICRF and the pixel variations, we calculate the IPRF for each pixel. Since the noise variation is not modelled in the pixel variation, we apply the IPRF to the noiseless input image obtained by a mean valued image of multiple shots to recover the scene radiance value for data cost modification.

For data costs, we utilize BT and NCC to compare the data costs in the intensity space, the



(a) Left Image

(b) Right Image

Figure 13. Bumblebee Stereo Data 4 - Projector set

image irradiance space, and the scene radiance space. BT is for comparison of  $L_p$  norm-based measure and NCC is for comparison of normalized measure which removes local variations such as lighting direction and specularity of objects in each space. Since we cannot remove lighting variations and specular effects up to the scene radiance space, NCC shows better results than BT even in the recovered scene radiance space.

To minimize the energy (6), we consider well-known optimization techniques such as Belief Propagation, Graph Cuts and their variations including BP-M, TRW-S,  $\alpha$ -expansion, and Log-Cut [22, 13]. Among them, we use TRW-S which is referred as the state-of-the-art energy minimization method [22].

The data sets used for our experiments are shown in Figs. 10- 13 and the corresponding stereo results are shown in Figs. 14- 17, respectively. Through the result of Bookshelf 1 set shown in Fig. 10, we can verify that the data cost in the scene radiance space shows better result than those in other spaces. In addition, since it is proven that the NCC cost shows better performance than BT cost in [11], we only compare the results of NCC for other data set to reduce redundant comparisons. The result of BT in the image irradiance space, Fig. 14(b), shows that the data cost using the ICRF without considering the linear function  $s(L)$  possibly degrades the result due to the non-negligible optical variations [20].

Since there is no accurate ground truth, we have to analyze the results in qualitative manner in the captions of each figure.



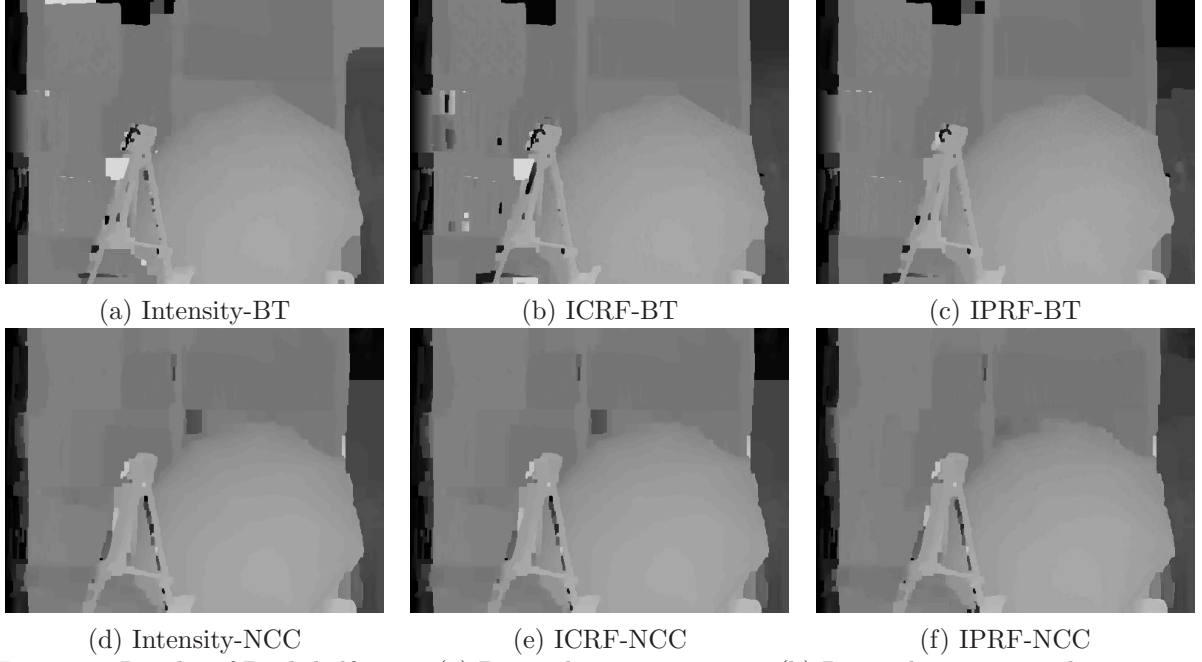


Figure 14. Results of Bookshelf 1 set. (a) BT in the intensity space (b) BT in the image irradiance space (c) BT in the scene radiance space. (d) NCC in the intensity space (e) NCC in the image irradiance space (f) NCC in the scene radiance space. In (c), The less error region than (a) is the right upper corner and the left below corner of tripod’s head. NCC shows better result than BT. In (f), The less error region is the center of the bookshelf and the right upper corner which has more homogeneous disparities.

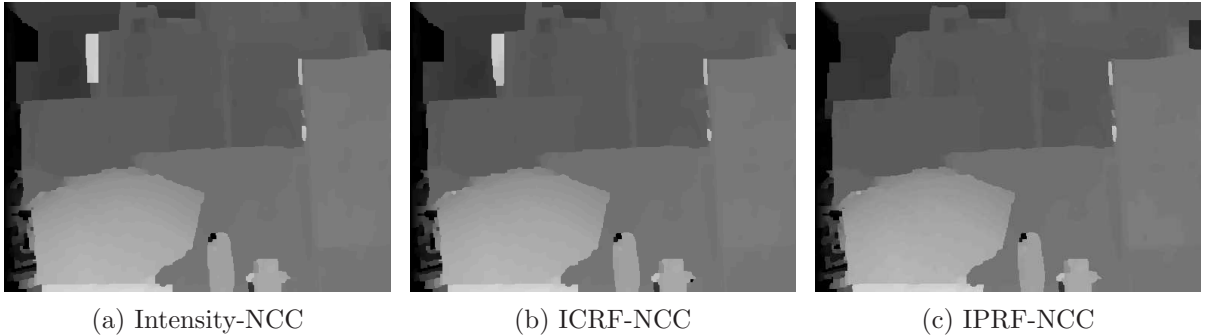


Figure 15. Results of Bookshelf 2 set. (a) NCC in the intensity space (b) NCC in the image irradiance space (c) NCC in the scene radiance space. In (c), The less error region is the upper mid-left side of the bookshelf region.

## 5. Conclusion

So far we have shown that the improved data costs in the scene radiance space by a direct radiometric calibration approach leads to better stereo matching results. Although the RRF is assumed to be spatially invariant previously, we verify this assumption should be revised by comparing the stereo matching result using the IRRF and the IPRF. Moreover, we successfully model the camera variation and the linear function by a single gain without loss of generality so that the resulting stereo disparity map is enhanced.

The recovered scene radiance value is possibly utilized by many vision applications. Since



(a) Intensity-NCC

(b) ICRF-NCC

(c) IPRF-NCC

Figure 16. Results of Photoboard set. (a) NCC in the intensity space (b) NCC in the image irradiance space (c) NCC in the scene radiance space. In (c), a large black hole in the right middle position is removed.



(a) Intensity-NCC

(b) ICRF-NCC

(c) IPRF-NCC

Figure 17. Results of Projector set. (a) NCC in the intensity space (b) NCC in the image irradiance space (c) NCC in the scene radiance space. In (c), a black hole in the projector body is removed.

the IPRF which is the function from an integer to real number value can recover the scene radiance value in floating point precision, the overall quality of super-resolution application can be accurately enhanced up to up to real number precision.

## References

- [1] <http://ee.columbia.edu/cave>, 2006. 4
- [2] <http://vision.middlebury.edu/stereo/>, 2006. 1
- [3] S. Birchfield and C. Tomasi. Depth discontinuities by pixel-to-pixel stereo, 1998. ICCV 1998. 10
- [4] P. Debevec and J. Malik. Recovering high dynamic range radiance maps from photographs, 1997. SIGGRAPH 1997. 3
- [5] O. Faugeras, B. Hotz, H. Mathieu, T. Vieville, Z. Zhang, P. Fua, E. Theron, L. Moll, G. Berry, J. Vuillemin, P. Bertin, and C. Proy. Real time correlation based stereo: algorithm implementations and applications, 1993. INRIA Technical Report 1993. 1
- [6] M. Gennert. Brightness-based stereo matching, 1988. ICCV 1988. 10
- [7] J. Gröbner, M. Blumthaler, and W. Ambach. Experimental investigation of spectral global irradiance measurement errors due to a non ideal cosine response, 1996. Geophysical Research Letters, Volume 23, Issue 18, p. 2493-2496. 8



- [8] M. D. Grossberg and S. Nayar. Modeling the space of camera response functions, 2004. PAMI 2004. [2](#), [3](#)
- [9] M. D. Grossberg and S. K. Nayar. What is the space of camera response functions?, 2003. CVPR 2003. [2](#), [3](#)
- [10] G. E. Healey and R. Kondepudy. Radiometric ccd camera calibration and noise estimation, 1994. PAMI 1994. [2](#), [3](#)
- [11] H. Hirschmuller and D. Scharstein. Evaluation of cost functions for stereo matching, 2007. CVPR 2007. [2](#), [5](#), [13](#)
- [12] J. Kim, V. Kolmogorov, and R. Zabih. Visual correspondence using energy minimization and mutual information, 2003. ICCV 2003. [1](#)
- [13] V. Lempitsky, C. Rother, and A. Blake. Logcut - efficient graph cut optimization for markov random fields, 2007. ICCV 2007. [13](#)
- [14] S. Lin, J. Gu, S. Yamazaki, and H. Shum. Radiometric calibration from a single image, 2004. CVPR 2004. [3](#)
- [15] S. Lin and L. Zhang. Determining the radiometric response function from a single grayscale image, 2005. CVPR 2005. [3](#)
- [16] C. Liu, W. T. Freeman, R. Szeliski, and S. B. Kang. Noise estimation from a single image, 2006. CVPR 2006. [6](#)
- [17] Y. Matsushita and S. Lin. A probabilistic intensity similarity measure based on noise distributions, 2007. CVPR 2007. [6](#)
- [18] Y. Matsushita and S. Lin. Radiometric calibration from noise distribution, 2007. CVPR 2007. [3](#), [6](#)
- [19] T. Mitsunaga and S. Nayar. Radiometric self calibration, 1999. CVPR 1999. [3](#), [9](#), [12](#)
- [20] S. A. Ramakrishna and J. B. Pendry. Removal of absorption and increase in resolution in a near-field lens via optical gain, 2003. PHYSICAL REVIEW B 67, 201101(R). [2](#), [6](#), [13](#)
- [21] D. Scharstein and R. Szeliski. A taxonomy and evaluation of dense two-frame stereo correspondence algorithms, 2002. IJCV 2002. [5](#), [11](#)
- [22] R. Szeliski, R. Zabih, D. Scharstein, O. Veksler, V. Kolmogorov, A. Agarwala, M. Tappen, and C. Rother. A comparative study of energy minimization methods for markov random fields, 2007. PAMI 2007. [13](#)
- [23] C.-C. Wang. A study of cmos technologies for image sensor applications, 2001. Ph.D Dissertation at M.I.T., 57 - 113. [2](#), [6](#)